Letter

Onset of uncontrolled polytypism during the Au-catalyzed growth of wurtzite GaAs nanowires

Wouter H. J. Peeters,[1,*] Marco Vettori,[1,*] Elham M. T. Fadaly,[1,*] Alexandre Danescu,[2,*] Chenyang Mao,[1] Marcel A. Verheijen,[1,3] and Erik P. A. M. Bakkers[1,†]

[1]*Department of Applied Physics, Eindhoven University of Technology, 5600 MB Eindhoven, The Netherlands*
[2]*University of Lyon, Lyon Institute of Nanotechnologies, UMR CNRS-5270, Ecole Centrale de Lyon, 69130 Ecully, France*
[3]*Eurofins Materials Science Netherlands BV, 5656 AE Eindhoven, The Netherlands*

(Received 7 November 2023; accepted 19 January 2024; published 27 February 2024)

The optoelectronic properties of a semiconductor are determined by the combination of its elemental composition and the crystal structure. The vapor-liquid-solid nanowire growth mechanism offers the controlled epitaxy of the zinc-blende and wurtzite polytype for a number of semiconductors. Long, thin, and phase-pure wurtzite GaAs nanowires are desirable as epitaxial templates for the growth of hexagonal SiGe shells, but the growth of such nanowires remains a challenge. Here, we study the growth of wurtzite GaAs nanowires and find a diameter dependent critical length beyond which the crystal phase becomes mixed. The onset of uncontrolled polytypism is modeled with a small contribution of As diffusion during growth. Due to this increased supply of As during prolonged growth, Ga is depleted from the liquid catalyst, thereby decreasing the contact angle. We investigate possible pathways of As through diffusion on the facets and edges of the nanowire, and from the scaling of the critical length we deduce that edge diffusion has an important contribution. This study offers new insights for realizing long, phase-pure wurtzite GaAs nanowires with high aspect ratio.

DOI: 10.1103/PhysRevMaterials.8.L020401

Introduction. Polytypism arises due to a small difference in the energy of formation of different crystal phases and has been observed in several materials. For instance, the cubic zinc blende (ZB) and hexagonal wurtzite (WZ) crystal phases can occur in group II–VI and III–V semiconductors [1]. The crystal polytype is a key factor in determining the optoelectronic properties [2], and crystal phase engineering has been proposed as a tool to realize new structures.

Group III–V semiconductor nanowires (NWs) offer an unprecedented level of control of the crystal phase. This opened new opportunities, such as quantum dots and tunnel barriers based on ZB/WZ homojunctions [3,4]. Recently, WZ GaP and GaAs NWs have been proposed as epitaxial templates for the growth of hexagonal (Hex) SiGe shells [5,6]. This application requires long and phase-pure WZ GaP and GaAs NWs, since the length of the WZ template dictates the length of the hexagonal segment. Yet, achieving long WZ GaAs NWs is challenging.

Theoretical studies [7] and *in situ* TEM measurements [8] show that formation of the WZ phase grown by the vapor-liquid solid (VLS) growth mechanism is driven by the contact angle of the catalyst at the triple-phase line. The catalyst contact angle can be tuned by the growth parameters such as the temperature and the V/III precursor ratio [9,10]. Apart from Au-catalyzed growth, it has been shown that WZ GaAs can also be formed in self-catalyzed NWs [11–13].

In this work, we investigate the time evolution of Au-catalyzed GaAs NWs with the aim to grow long and phase-pure WZ GaAs. We find that axial growth beyond a critical length (L_{cr}) results in a mixed-phase crystal. The critical length increases with the diameter of the NW, and it is thus more difficult to grow WZ GaAs NWs with a small diameter. We interpret the critical length as the consequence of increased arsenic (As) capture. The increased As supply depletes the catalyst from gallium (Ga), thereby affecting the contact angle and the NW crystal structure. These insights increase our understanding of the NW growth mechanism and are essential to fully exploit crystal phase engineering of GaAs NWs.

Epitaxy of wurtzite gallium arsenide. Arrays of GaAs NWs are grown from Au catalysts, defined by e-beam lithography, using metal organic vapor phase epitaxy (MOVPE) growth conditions optimized for the formation of the WZ structure (See the Methods section of the Supplemental Material [14]). In the scanning electron microscopy (SEM) images of Fig. 1, samples with a different growth time are compared. For a relatively short growth time of one hour, [Fig. 1(a)], both the top and bottom parts of the NW have the WZ crystal structure, as confirmed by transmission electron microscopy (TEM) in Fig. 1(c). In this case, the diameter of the NW is equal near the bottom and the top. The absence of tapering indicates that there is no radial growth on the $\{10\bar{1}0\}$ facets of the NW. The contact angle of the catalyst is approximately 90°, which is in agreement with the observed WZ crystal structure below the droplet [8]. In contrast, after an extended growth duration of five hours, the contact angle is larger than 90° as shown in Fig. 1(d). The larger contact angle is related to a smaller NW diameter below the droplet, where the crystal is mixed phase as visible from the high density of stacking faults near the top. Yet, the bottom of the NW is WZ, indicating that a transition from WZ to mixed phase occurs for constant growth conditions. We define the length at which the NW turns from WZ to mixed phase as the critical length.

*These authors contributed equally to this work.
†e.p.a.m.bakkers@tue.nl

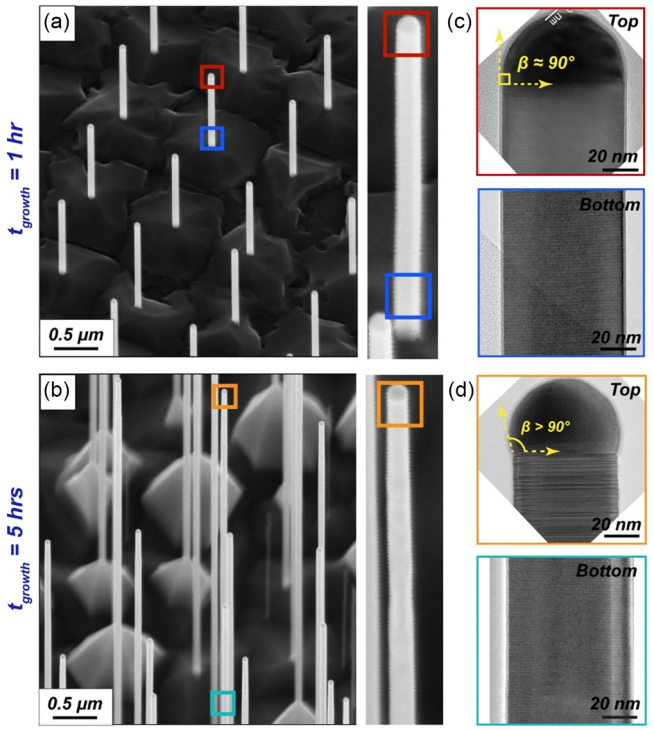

FIG. 1. (a), (b) SEM images of NW arrays with the same diameter ($D = 80$ nm), grown for one hour or five hours, respectively. The right panel shows an enlarged view of a single NW from both panels. The colored boxes correspond to regions studied in TEM. (c), (d) Bright field TEM images in the [11$\bar{2}$0] zone axis. Short WZ NWs show no tapering, a WZ crystal phase, and a contact angle of approximately 90°. In contrast, long NWs show a mixed phase at the top. The contact angle is larger than 90° related to to a shrinking NW diameter at the top.

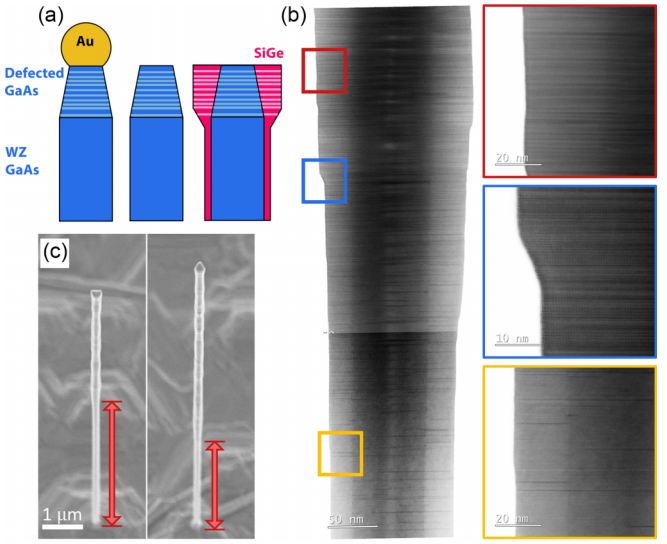

FIG. 2. (a) Schematic representation of the approach to determine the critical length. First, the Au droplet is chemically etched from the GaAs, after which a Hex $Si_{0.2}Ge_{0.8}$ shell is deposited. The shell is thicker on the mixed-phase part due to an increased growth rate. (b) Bright field TEM images around the transition from WZ to mixed-phase core. The NW has the hexagonal crystal structure with I3 defects in the shell below the critical length (yellow). Both core and shell are mixed-phase above the critical length (red). Narrow bands of hexagonal stacking are visible where the diameter increases (blue). (c) SEM images of NWs after deposition of a Hex $Si_{0.2}Ge_{0.8}$ shell; the measured critical length based on the shell thickness is indicated.

Measurement of the critical length. The transition from WZ to mixed phase can be observed with TEM. For the TEM analysis the NWs have to be broken off from the substrate. However, breaking the NWs is an uncontrolled process, where the NW is broken at a random point, partly due to the varying parasitic growth around the base of each NW [Fig. 1(b)]. We, therefore, develop a new method to determine the critical length as a function of NW diameter.

The approach we used to measure the critical length is illustrated in Fig. 2(a). After the chemical etching of the Au droplet, a $Si_{0.2}Ge_{0.8}$ shell is radially grown around the GaAs NW (see the Methods section of the Supplementa Material [14]). The SiGe shell copies the crystal structure of the GaAs template. Importantly, the radial growth rate depends on the crystal structure. The $Si_{0.2}Ge_{0.8}$ growth rate is higher on the mixed-phase GaAs compared to the WZ GaAs, which is shown in Fig. 2(b). The $Si_{0.2}Ge_{0.8}$ adopts the hexagonal crystal structure where the core is wurtzite. The shell is hexagonal with some partial I3 stacking faults [15], as shown in the yellow inset. Above the critical length, both core and shell are mixed phase (red inset). The diameter of the shell increases in the transition zone between the WZ and mixed-phase region of the core. The transition zone is characterized by narrow bands of hexagonal stacking in the shell (blue inset). The increased diameter of the shell can be observed in SEM, as illustrated in Fig. 2(c). For each GaAs NW diameter, between 13 and 30 NWs were characterized using SEM to determine the critical length. The difference in critical length between NWs with the same core diameter is larger than the spread induced by the gradual diameter increase in the transition zone. Hence, this is a valid method to obtain statistical data of the critical length.

The correlation between the critical length and the GaAs NW diameter is shown in Fig. 3. We determined the critical length for four different diameters, while NWs with diameters above 120 nm have not reached the critical length even for the longest growth duration used, and are wurtzite until at least 15 μm. Determining the critical length for longer NWs is challenging due to the limited mechanical stability of the NWs during the wet-chemical Au removal process. Based on Fig. 3 it can be concluded that the critical length increases with the GaAs NW diameter. A model is developed to unveil the underlying mechanism.

Modeling the critical length. A number of important experimental observations are discussed to understand the growth dynamics of WZ GaAs NWs. First, the diameter of the WZ NWs is determined by the size of the Au catalyst, and the diameter does not increase with growth time (see Fig. S2 of the Supplemental Material [14]). Thus, the axial growth rate dominates the growth, with negligible radial growth. Second, the axial growth rate is independent of the pitch, as investigated for interwire spacings between 250 nm and 3 μm (see

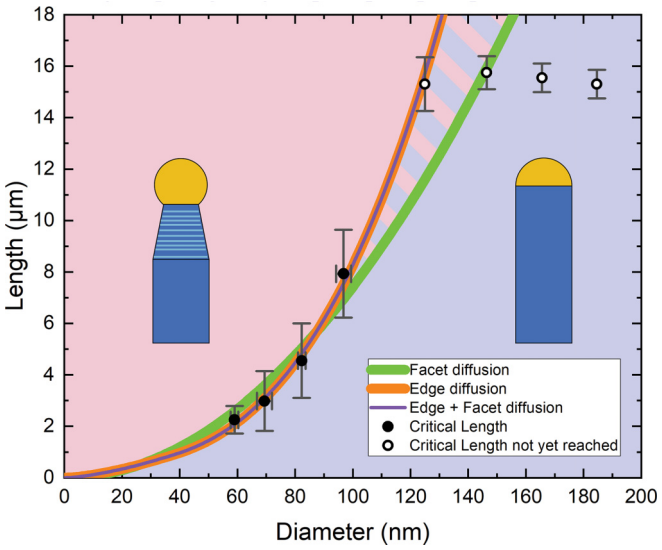

FIG. 3. Length of the wurtzite segment in the GaAs NWs, measured by SEM. The wurtzite length increases with the diameter of the GaAs NWs (closed circles). No transition toward mixed phase was observed above a diameter of 120 nm for the longest growth time probed (open circles). Vertical error bars represent the standard deviation of length between different NWs. The data is fitted with a model containing only facet diffusion (green line), only edge diffusion (orange line), or a combination of facet and edge diffusion (purple line). Combinations of diameter and length where the NWs are WZ or mixed phase are highlighted in blue and red, respectively. The dashed region highlights the disagreement between the models.

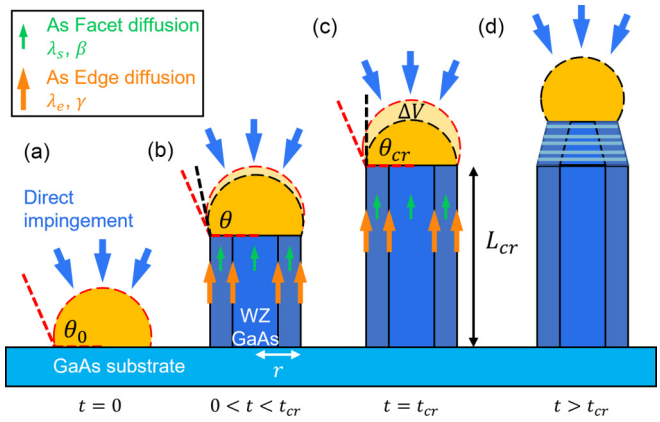

FIG. 4. Proposed time evolution of the NW growth until the critical length. (a) Au-Ga eutectic with initial contact angle θ_0 on the GaAs substrate. Axial growth is due to direct impingement of Ga and As precursors on the droplet (blue arrows). (b) Supply of As through facet and edge diffusion decreases the catalyst volume (black dashed lines) compared to the initial catalyst (red dashed lines). Thus, $\theta < \theta_0$. (c) The NW has reached the the critical length L_{cr}. Arsenic diffusion resulted in a total decrease of the catalyst volume ΔV due to a consumption of Ga. Consequently, the contact angle decreased to θ_{cr}. (d) Growth beyond the critical length. The contact angle is too large, leading to nucleation of mixed-phase GaAs.

Fig. S3 of the Supplemental Material [14]). This implies that diffusion of adatoms on the substrate surface towards the Au droplet is not limiting the axial growth [16]. Third, the axial growth rate of the NWs does not change with growth time and is diameter independent, as long as the critical length has not yet been reached (see Fig. S4 of the Supplemental Material [14]). The diameter- and NW length-independent growth rate both imply that the growth rate is not influenced by the size of the sidefacets, i.e., the capture area for the diffusion of adatoms. Thus, the diffusion of Ga on the sidewalls does not contribute significantly to the axial growth of WZ GaAs [16]. Above the critical length the growth rate is diameter dependent, and thin wires grow faster (see Fig. S5 of the Supplemental Material [14]). The increased axial growth rate of mixed-phase GaAs, combined with the smaller NW diameter near the top [Fig. 1(d), indicates a compensation mechanism to keep the volumetric growth rate approximately constant.

The combination of the above observations implies a growth regime where the axial growth is mainly through direct impingement of precursors on the Au catalyst [16,17]. We develop a model considering a mass-transport limited mechanism for the growth of WZ GaAs. The equal amount of Ga and As atoms entering the liquid droplet of an 80 nm diameter NW that grows at a constant axial growth rate of 0.5 nm/s (see Fig. S5 of the Supplemental Material [14]) is $4.34 \cdot 10^4$ atoms/sec. The volume of the catalyst, and thus its contact angle, is mainly defined by the amount of Ga atoms, due to the limited solubility of As in Au [18]. The deficit of Ga atoms leading to a decrease of the droplet volume from an initial wetting angle of 95° to a critical wetting angle of 90° [7] is about $3.77 \cdot 10^5$ atoms. The catalyst volume decreases during several hours of the growth process, while it corresponds to the amount of Ga needed for approximately nine seconds of axial NW growth. This lead us to conclude that there are two processes occurring at different time scales. First, there is a dominant amount of equal quantities entering the droplet by direct impingement resulting in the axial growth at constant growth rate. The second process is a small perturbation of additional As entering the droplet via either surface diffusion along the NW facets and/or line diffusion along the NW edges. This small amount of additional As entering the droplet through NW surface/line diffusion contributes with a negligible quantity to the axial growth rate. However, it is responsible for the slow reduction of the Ga amount in the droplet, triggering the transition between the pure WZ segment to the mixed-phase segment when the critical wetting angle of 90° is reached after prolonged growth (Fig. 4). The diffusion of volatile group V species is still a topic of debate for molecular beam epitaxy (MBE). The diffusion is usually estimated to be negligible [19], however, it has also been considered to explain several scenarios where it may have a significant contribution [20,21]. In what follows, we discuss the qualitative and the quantitative aspects of As diffusion in MOVPE, where we believe it is responsible for the transition from pure WZ phase to a mixed-phase growth.

In a generic setting, if r, θ_0, and θ_{cr} denote the NW radius, the initial wetting angle and the critical wetting angle (hereafter 90° [7]), respectively, the amount of Ga adatoms involved in the droplet volume decrease is given by

$$Q_{Ga} = \alpha \Delta V = \alpha \pi r^3 \Delta f, \quad (1)$$

where $\alpha = 54.35$ atoms/nm^3 is a density conversion factor, and $\Delta f = f(\theta_0) - f(\theta_{\rm cr})$, with

$$f(\theta) = \frac{(2+\cos\theta)(1-\cos\theta)^2}{3\sin^3\theta}. \tag{2}$$

The expression $\pi r^3 f(\theta)$ describes the volume of the spherical cap droplet located at the top of a cylindrical NW with radius r as a function of the wetting angle θ. If the droplet volume decrease ΔV is due to additional As entering the droplet through surface diffusion we can relate the critical length ($L_{\rm cr}$) to the NW radius as follows: let λ_s denote the surface-diffusion length of As species along the NW facets. Then, if $L_{\rm cr} \leqslant \lambda_s$, the amount of As entering the droplet along the growth process up to the critical length is

$$Q_{As} = 6r\beta \int_0^{t_{\rm cr}} L(\tau)d\tau = 3r\beta V_{ax} t_{\rm cr}^2 = \frac{3r\beta}{V_{ax}} L_{\rm cr}^2, \tag{3}$$

where β is the amount of atoms per unit surface in unit time and, as the axial growth rate is constant, $L(\tau) = V_{ax}\tau$ so that $t_{\rm cr} = L_{\rm cr}/V_{ax}$. By comparing (1) and (3) we obtain a linear scaling $L_{\rm cr} = kr$ with a slope given by the dimensionless quantity $k = (\frac{\alpha\pi}{3\beta} V_{ax}\Delta f)^{1/2}$.

If the critical length is instead larger than the diffusion length ($L_{\rm cr} > \lambda_s$), then the growth process has to be divided in two sequential stages. Starting with $L(\tau) \leqslant \lambda_s$, where the capture area for As diffusion is limited by the NW length, followed by $L(\tau) \geqslant \lambda_s$, where there is a constant supply of As from surface diffusion. The total amount of As that diffused to the droplet can then be written as the sum of two integrals

$$\begin{aligned} Q_{As} &= 6r\beta\left(\int_0^{t_s} L(\tau)d\tau + \int_{t_s}^{t_{\rm cr}} \lambda_s d\tau\right) \\ &= \frac{6r\beta}{V_{ax}}\left(\lambda_s L_{\rm cr} - \frac{1}{2}\lambda_s^2\right), \end{aligned} \tag{4}$$

where we introduced $t_s = \lambda_s/V_{ax}$, the growth time necessary to reach the diffusion length λ_s. Equation (4) combined with (1) gives a quadratic dependence between $L_{\rm cr}$ and r. Collecting together (3) and (4) we obtain an equation for the critical length due to surface diffusion of As,

$$L_{\rm cr}(r) = \begin{cases} kr & \text{for} \quad kr \leqslant \lambda_s \\ r^2\frac{k^2}{2\lambda_s} + \frac{\lambda_s}{2} & \text{for} \quad kr \geqslant \lambda_s. \end{cases} \tag{5}$$

The relation involves two parameters, λ_s and k, to be determined from the experimental data.

We remark that the quadratic dependence r^2 on the second line in (5) can be understood based on dimensionality. The consumed volume of Ga scales with r^3, while the surface diffusion only scales with r, and the discrepancy results in the quadratic dependence. If instead of surface diffusion we introduce line diffusion along the NW edges, i.e., a radius-independent channel, then a piecewise function with a cubic branch is obtained. The diffusion on the edges is described with an edge diffusion length λ_e and by replacing $r\beta$ with γ [in atoms/(nm· s)] in (3) and (4), giving

$$L_{\rm cr}(r) = \begin{cases} \hat{k}r^{3/2} & \text{for} \quad \hat{k}r^{3/2} \leqslant \lambda_e \\ r^3\frac{\hat{k}^2}{2\lambda_e} + \frac{\lambda_e}{2} & \text{for} \quad \hat{k}r^{3/2} \geqslant \lambda_e, \end{cases} \tag{6}$$

where now $\hat{k}^2 = \frac{\alpha\pi}{3\gamma} V_{ax}\Delta f$ (in nm^{-1}) is the inverse of a characteristic length.

Experimentally, both diffusion on the facets and edges could contribute to the deficit of Ga in the droplet. The combination of these mechanisms requires a wider discussion of the relative positions of $L_{\rm cr}$, λ_s, and λ_e. For instance, the particular case when $\lambda_e = \lambda_s = \lambda_{e/s}$ gives

$$L_{\rm cr}(r) = \begin{cases} k\left(\frac{r^3}{r+\hat{\gamma}}\right)^{1/2} & \text{for} \quad k^2\frac{r^3}{r+\hat{\gamma}} \leqslant \lambda_{e/s}^2 \\ \frac{r^3}{r+\hat{\gamma}}\frac{k^2}{2\lambda_{e/s}} + \frac{\lambda_{e/s}}{2} & \text{for} \quad k^2\frac{r^3}{r+\hat{\gamma}} \geqslant \lambda_{e/s}^2, \end{cases} \tag{7}$$

where $\hat{\gamma} = \gamma/\beta = k^2/\hat{k}^2$ is a characteristic length. A complete discussion of the generic situation ($\lambda_e \neq \lambda_s$) is presented in Sec. III A in the Supplemental Material [14].

The four critical length points between diameters of 60 and 100 nms are fitted with the three different models, and the identification procedure for the best fit to the experimental data is presented in detail in Sec. III B in th Supplemental Material [14]. Using the piecewise expression for As surface diffusion in (5) one obtains $k = 0.5$ and $\lambda_s = 4.2 \cdot 10^{-5}$ μm. We consider this a nonphysical result, since the diffusion length is less than a single monolayer. In contrast, using (6) for As diffusion on the edges and the experimental data we obtain $\lambda_e = 0.94$ μm and $\hat{k} = 342.8$ (μm)$^{-1/2}$ which is both physically acceptable and stable (see Sec. III B in the Supplemental Material [14]) with respect to initial conditions. Moreover, using the more general expression (7) we again obtain $\lambda_{e/s} = 0.94$ μm, while for k and $\hat{\gamma}$ we notice a strong dependence on the initial data in the fit procedure (see Sec. III B in the Supplemental Material [14]). This behavior can be explained as follows: a good fit is obtained for values of $\hat{\gamma}$ of order 10^2 and this means that in the second line of (7) the $r + \hat{\gamma}$ term is dominated by $\hat{\gamma}$. It follows that one can obtain only the ratio $\hat{k}^2/\hat{\gamma}$ or, otherwise stated, a scaling of the parameters $(\hat{\gamma}, \hat{k}) \to (\alpha^2\hat{\gamma}, \alpha\hat{k})$ will provide the same fit. The physical meaning of this nonunique result, due to a high $\hat{\gamma}$ for the best fit, is that edge diffusion dominates surface diffusion. The fits of the three different models are presented in Fig. 3. The surface diffusion model (in green) predicts a critical length around 10.5 μm for a diameter of 120 nm, which is in disagreement with experimental observation. The edge diffusion model (in orange) fits better to the four critical length points. Additionally, it correctly predicts the WZ phase with a diameter of 120 nm. The model including both surface and edge diffusion (in purple) is not distinguishable from edge diffusion only. Thus, only considering an edge diffusion mechanism gives a good estimate of the observed critical length.

Edge diffusion is a mechanism which is typically not considered, and further studies are necessary to see if edge diffusion manifests itself in other material systems and geometries. Other causes for the critical length have been considered, being (i) imbalance of the V/III ratio in the close environment of the catalyst particle, (ii) change of temperature near the catalyst particle [22], (iii) competitive parasitic growth, and (iv) the Gibbs-Thomson effect [23,24], but these mechanisms cannot explain all of the experimental observations (see Sec. III C in the Supplemental Material [14]). Possibly, the edge diffusion channels are physically represented as small $\{11\bar{2}0\}$ facets on the NWs. Indeed, the

diffusion constant along [0001] of As surface species has been predicted to be larger on the $\{11\bar{2}0\}$ facets compared to the $\{10\bar{1}0\}$ facets [25].

The model predicts that the As excess through diffusion can be neutralized by additional Ga supply. This supply can be either continuous, by changing the V/III ratio during growth, or pulsed, by shortly increasing the supply of Ga relative to As. The continuous supply of more Ga is especially interesting once the NW length is longer than the diffusion length of As ($\lambda_e = 0.94$ μm). Then, a small amount of added Ga in the gas phase can counteract the As entering the droplet through diffusion. These experiments are the subject of future investigations. Here, we show some preliminary result of additional Ga supply through pulses (see Sec. IV in the Supplemental Material [14]). Short Ga pulses during growth can inflate the droplet, preventing it from going below the critical contact angle of 90°. However, the length of the Ga pulse should be carefully chosen. Overexposure to Ga will inflate the catalyst beyond the contact angle necessary for WZ growth, resulting in the nucleation of mixed phase as well. Utilizing Ga pulses may result in WZ GaAs NWs beyond the critical length presented in this manuscript. The experiments with Ga pulses presented in Sec. IV in the Supplemental Material [14] confirm that the critical length is due to a shortage of Ga in the catalyst.

Conclusion. We observed a transition from WZ to mixed phase for GaAs NW growth. The length at which this transition occurs increases with the diameter of the NW. The diameter dependence is best described by diffusion of As species on the edges of the NW.

Acknowledgments. We acknowledge financial support from the EU through H2020-FETOpen project OptoSilicon (Grant Agreement No. 964191). We thank P. J. van Veldhoven and M. G. van Dijstelbloem for the technical support of the MOVPE reactor. We furthermore acknowledge the Dutch province of Noord-Brabant for funding the TEM facility.

[1] C.-Y. Yeh, Z. W. Lu, S. Froyen, and A. Zunger, Zinc-blende–wurtzite polytypism in semiconductors, Phys. Rev. B **46**, 10086 (1992).

[2] F. Bechstedt and A. Belabbes, Structure, energetics, and electronic states of III–V compound polytypes, J. Phys.: Condens. Matter **25**, 273201 (2013).

[3] N. Akopian, G. Patriarche, L. Liu, J.-C. Harmand, and V. Zwiller, Crystal phase quantum dots, Nano Lett. **10**, 1198 (2010).

[4] K. A. Dick, C. Thelander, L. Samuelson, and P. Caroff, Crystal phase engineering in single InAs nanowires, Nano Lett. **10**, 3494 (2010).

[5] H. I. T. Hauge, M. A. Verheijen, S. Conesa-Boj, T. Etzelstorfer, M. Watzinger, D. Kriegner, I. Zardo, C. Fasolato, F. Capitani, P. Postorino *et al.*, Hexagonal silicon realized, Nano Lett. **15**, 5855 (2015).

[6] E. M. T. Fadaly, A. Dijkstra, J. R. Suckert, D. Ziss, M. A. van Tilburg, C. Mao, Y. Ren, V. T. van Lange, K. Korzun, S. Kölling *et al.*, Direct-bandgap emission from hexagonal Ge and SiGe alloys, Nature (London) **580**, 205 (2020).

[7] F. Glas, J.-C. Harmand, and G. Patriarche, Why does wurtzite form in nanowires of III-V zinc blende semiconductors? Phys. Rev. Lett. **99**, 146101 (2007).

[8] D. Jacobsson, F. Panciera, J. Tersoff, M. C. Reuter, S. Lehmann, S. Hofmann, K. A. Dick, and F. M. Ross, Interface dynamics and crystal phase switching in GaAs nanowires, Nature (London) **531**, 317 (2016).

[9] H. J. Joyce, J. Wong-Leung, Q. Gao, H. H. Tan, and C. Jagadish, Phase perfection in zinc blende and wurtzite III-V nanowires using basic growth parameters, Nano Lett. **10**, 908 (2010).

[10] S. Lehmann, D. Jacobsson, and K. A. Dick, Crystal phase control in GaAs nanowires: Opposing trends in the Ga-and As-limited growth regimes, Nanotechnology **26**, 301001 (2015).

[11] M. M. Jansen, P. Perla, M. Kaladzhian, N. von den Driesch, J. Janssen, M. Luysberg, M. I. Lepsa, D. Grützmacher, and A. Pawlis, Phase-pure wurtzite GaAs nanowires grown by self-catalyzed selective area molecular beam epitaxy for advanced laser devices and quantum disks, ACS Appl. Nano Mater. **3**, 11037 (2020).

[12] T. Dursap, M. Vettori, C. Botella, P. Regreny, N. Blanchard, M. Gendry, N. Chauvin, M. Bugnet, A. Danescu, and J. Penuelas, Wurtzite phase control for self-assisted GaAs nanowires grown by molecular beam epitaxy, Nanotechnology **32**, 155602 (2021).

[13] F. Panciera, Z. Baraissov, G. Patriarche, V. G. Dubrovskii, F. Glas, L. Travers, U. Mirsaidov, and J.-C. Harmand, Phase selection in self-catalyzed GaAs nanowires, Nano Lett. **20**, 1669 (2020).

[14] See Supplemental Material at http://link.aps.org/supplemental/10.1103/PhysRevMaterials.8.L020401 for additional information regarding the methods, growth kinetics, fitting procedure and Ga-pulsing experiments.

[15] E. M. T. Fadaly, A. Marzegalli, Y. Ren, L. Sun, A. Dijkstra, D. De Matteis, E. Scalise, A. Sarikov, M. De Luca, R. Rurali *et al.*, Unveiling planar defects in hexagonal group IV materials, Nano Lett. **21**, 3619 (2021).

[16] J. Johansson, C. P. T. Svensson, T. Mårtensson, L. Samuelson, and W. Seifert, Mass transport model for semiconductor nanowire growth, J. Phys. Chem. B **109**, 13567 (2005).

[17] V. G. Dubrovskii, G. E. Cirlin, I. P. Soshnikov, A. A. Tonkikh, N. V. Sibirev, Y. B. Samsonenko, and V. M. Ustinov, Diffusion-induced growth of GaAs nanowhiskers during molecular beam epitaxy: Theory and experiment, Phys. Rev. B **71**, 205325 (2005).

[18] C. B. Maliakkal, D. Jacobsson, M. Tornberg, A. R. Persson, J. Johansson, R. Wallenberg, and K. A. Dick, In situ analysis of catalyst composition during gold catalyzed GaAs nanowire growth, Nat. Commun. **10**, 4577 (2019).

[19] M. R. Ramdani, J. C. Harmand, F. Glas, G. Patriarche, and L. Travers, Arsenic pathways in self-catalyzed growth of GaAs nanowires, Cryst. Growth Des. **13**, 91 (2013).

[20] A. Pishchagin, F. Glas, G. Patriarche, A. Cattoni, J.-C. Harmand, and F. Oehler, Dynamics of droplet consumption in vapor–liquid–solid III–V nanowire growth, Cryst. Growth Des. **21**, 4647 (2021).

[21] D. Rudolph, S. Hertenberger, S. Bolte, W. Paosangthong, D. Spirkoska, M. Döblinger, M. Bichler, J. J. Finley, G. Abstreiter,

and G. Koblmüller, Direct observation of a noncatalytic growth regime for GaAs nanowires, Nano Lett. **11**, 3848 (2011).

[22] M. Raya-Moreno, R. Rurali, and X. Cartoixà, Thermal conductivity for III-V and II-VI semiconductor wurtzite and zinc-blende polytypes: The role of anharmonicity and phase space, Phys. Rev. Mater. **3**, 084607 (2019).

[23] V. G. Dubrovskii, N. V. Sibirev, G. E. Cirlin, I. P. Soshnikov, W. H. Chen, R. Larde, E. Cadel, P. Pareige, T. Xu, B. Grandidier, J.-P. Nys, D. Stievenard, M. Moewe, L. C. Chuang, and C. Chang-Hasnain, Gibbs-Thomson and diffusion-induced contributions to the growth rate of Si, InP, and GaAs nanowires, Phys. Rev. B **79**, 205316 (2009).

[24] L. E. Fröberg, W. Seifert, and J. Johansson, Diameter-dependent growth rate of InAs nanowires, Phys. Rev. B **76**, 153401 (2007).

[25] V. Pankoke, S. Sakong, and P. Kratzer, Role of sidewall diffusion in GaAs nanowire growth: A first-principles study, Phys. Rev. B **86**, 085425 (2012).